metals

Article

Evaluating Microstructure, Wear Resistance and Tensile Properties of Al-Bi(-Cu, -Zn) Alloys for Lightweight Sliding Bearings

Rodrigo André Valenzuela Reyes [1], Amauri Garcia [2] and José Eduardo Spinelli [1,3,*]

[1] Graduate Program in Materials Science and Engineering, Federal University of São Carlos, 13565-905 São Carlos, Brazil; rodrigoavreyes@gmail.com
[2] Department of Manufacturing and Materials Engineering, University of Campinas, UNICAMP, 13083-860 Campinas, Brazil; amaurig@fem.unicamp.br
[3] Department of Materials Engineering, Federal University of São Carlos, UFSCar, 13565-905 São Carlos, Brazil
* Correspondence: spinelli@ufscar.br; Tel.: +55-16-3351-8512

Abstract: One of the most important routes for obtaining Al-Bi-x monotectic alloys is directional solidification. The control of the thermal solidification parameters under transient heat flow conditions can provide an optimized distribution of the Bismuth (Bi) soft minority phase embedded into an Al-rich matrix. In the present contribution, Al-Bi, Al-Bi-Zn, and Al-Bi-Cu alloys were manufactured through this route with their microstructures characterized and dimensioned based on the solidification cooling rates. The main purpose is to evaluate the influence of typical hardening elements in Al alloys (zinc and copper) in the microstructure, tensile properties, and wear of the monotectic Al-Bi alloy. These additions are welcome in the development of light and more resistant alloys due to the growing demands in new sliding bearing designs. It is demonstrated that the addition of 3.0 wt.% Cu promotes microstructural refining, doubles the wear resistance, and triples the tensile strength with some minor decrease in ductility in relation to the binary Al-3.2 wt.% Bi alloy. With the addition of 3.0 wt.% Zn, although there is some microstructural refining, little contribution can be seen in the application properties.

Keywords: Al-Bi alloys; solidification; microstructure; wear; tensile properties

Citation: Valenzuela Reyes, R.A.; Garcia, A.; Spinelli, J.E. Evaluating Microstructure, Wear Resistance and Tensile Properties of Al-Bi(-Cu, -Zn) Alloys for Lightweight Sliding Bearings. *Metals* **2021**, *11*, 153. https://doi.org/10.3390/met11010153

Received: 23 December 2020
Accepted: 9 January 2021
Published: 15 January 2021

1. Introduction

Manufacture and metallurgical characteristics of immiscible Al-Bi binary alloys have been extensively investigated over the past 20 years [1–7]. Some restrictions have been reported. The main one is the difficulty of obtaining a uniform dispersion of the soft phase, i.e., the Bi. Even in the face of this aspect, interest in the development of Al-Bi and Al-Bi-X alloys is growing due to the potential of these alloys as advanced bearing materials, thanks to their self-lubricating property [6,7]. Other application possibilities are use as electrical contact materials, the fabrication of porous materials, and fuel cells [6–8].

Although it is difficult to achieve, a dispersive distribution of the minority phase can be reached through some manufacturing routes. The major routes in this matter are directional solidification [9,10], rapid cooling from the melt [11,12], and high static magnetic field [13,14].

Specifically, in the case of directional solidification, the control of thermal solidification parameters, such as cooling rate and growth rate, can be beneficial for the formation of homogeneously distributed minority phases. Silva et al. [9] demonstrated, by means of the application of directional solidification, that a very fine dispersion of Bi droplets with a diameter around 600 nm in the Aluminum (Al) matrix is obtained for growth rates, v, of 1 mm/s.

The directional solidification, therefore, is characterized as a promising route, including the control of other aspects of interest in the alloys development. For example, the morphology of the minority phase is also a very important aspect either in the distribution of that phase or in the variation of the resulting application properties of the alloy. Silva et al. [15] synthesized the influence of 'v' in the Pb-rich phase morphology of the immiscible Al-0.9 wt.% Pb alloy as follows: Pb droplets for v higher than 1.0 mm/s and Pb fibers for v lower than 0.65 mm/s.

In addition to the distribution of the soft phase in the microstructure, which is essential in achieving the self-lubricating effect, the achievement of suitable tensile properties is also necessary. These two factors become predominant in the development of advanced bearings. Sliding bearings are employed in car engines since they can provide a distribution of the applied load over a relatively wide area. They supplant the rolling bearings, which cannot withstand under the loading conditions of internal combustion engines [16–18]. The increase in the contact area and the high loads involved require satisfactory application properties of the sliding bearings. Because of that, sliding bearings for car engines are mostly based on the Cu-Sn bronze. In this regard, for the application of lightweight Al-based monotectic alloys to be viable, fine dispersion of soft particles in conjunction with a strong Al-based matrix become necessary. Additions of Zinc (Zn) [19], Copper (Cu) [20], and Silicon (Si) [21] can promote solid solution hardening of the Al matrix, making the matrices stronger.

In recent years, there has been an increase in the number of investigations regarding the addition of third elements [22–24] in monotectic alloys. Most of them emphasize the effects of these elements in restricting or not the segregation of the minority phase during solidification. However, there is a lack of research dedicated to surveying the impact of third elements on application properties of Al-Bi alloys, such as wear, corrosion, and mechanical strength.

The addition of Cerium [22], Lanthanum [23], or Neodymium [24] resulted in microstructural refinement of the Al-Bi alloys. In these three cases, particles containing the added element are formed in contact with the Bi globules, which provide an increase in the nucleation rate of the minority phase.

Yang and collaborators [25] investigated the effects of discrete additions of Tin (Sn), Cu and Si to a hypermonotectic Al-Bi alloy on the microstructure and mechanical properties. It has been shown that, due to the improved distribution via the ternary eutectic reaction, Sn facilitated refinement of the Bi-rich minority phase, while Si and Cu induced the reverse, resulting in coarsening of the Bi phase. In addition, the mechanical properties were greatly improved by alloying with Si and Cu (1.0 wt. per cent of each).

Pereira et al. [26] recently demonstrated that the tensile properties of the Al-15 wt.% Si-1 wt.% Bi alloy are higher than those of the non-modified Al-15 wt.% Si alloy. It is demonstrated that the addition of Bi to hypereutectic Al-Si alloys facilitates improvement in alloy strength. The formation of lamellar Si rather than flaky Si structure is the main explanation for this. In addition, Bi was attributed to prevent the propagation of cracks through the grain boundaries of the α-Al phase, minimizing the premature fracturing of the Si particles.

There is a lack of evidence on studies of Zn or Cu being applied to the monotectic Al-Bi alloys. For these systems, microstructural developments and their relationships to application properties remain unknown. The reason for the use of these elements lies in the ability to boost mechanical strength, while retaining the self-lubricating properties of Bi. The prospect of the Al-Bi alloys acting as advanced bearing alloys could become more feasible if these requirements are accomplished.

The experiments in the present work were conducted through upward transient directional solidification. The same analyzes used for the ternary Al-Bi-Cu and Al-Bi-Zn alloys were also replicated in the binary Al-Bi alloy, with the latter serving as benchmark results. The solidification system used allows the identification of several microstructures depending on the variation in the cooling rate. In order to determine the main evolution of the Bi spacing, quantitative measurements along the axial length of the directionally solidified (DS) castings were performed. Tensile and wear tests were performed on samples whose Bi spacing was determined in advanced.

The present study aims at understanding the impact of discrete adding of 3 wt.% Cu and 3 wt.% Zn on the tensile properties and wear resistance of the monotectic Al-3.2 wt.% Bi alloy. In addition, the effects of these additions on the length scale and distribution of the soft Bi phase in the formed microstructures are evaluated. The experimental interrelationships between the wear resistance, tensile properties, and Bi spacing of the three alloys will be detailed.

2. Materials and Methods

Three monotectic alloys of interest were subjected to directional solidification experiments: Al-3.2 wt.% Bi, Al-3.2 wt.% Bi-3.0 wt.% Zn, and Al-3.2 wt.% Bi-3.0 wt.% Cu alloys. Compositions of Al, Bi and Zn used to prepare these alloys are shown in Table 1. Cu is not listed due to its 99.999% high purity as an electrolytic product. This experimental system is constructed so that, during transient solidification, cooling curves can be acquired. Microstructures and their Bi spacing and Bi diameter values correlated with a variety of sections from the base towards the top of each casting could be measured after solidification.

Table 1. Chemical compositions (wt.%) of metals used to prepare the Al-Bi(-X) alloys.

Elements (wt.%)	Al	Zn	Bi	Cu	Fe	Si	Sn	Cd	Pb	As	Sb
Al	99.85	0.01	-	-	0.09	0.05	-	-	-	-	-
Zn	0.0001	99.997	-	0.0002	0.0001	-	0.0001	0.0006	-	-	-
Bi	-	0.0005	99.99	0.0005	0.001	-	0.001	0.0005	0.001	0.001	0.0005

The scheme in Figure 1 includes all the key elements associated with the directional solidification technique used in the present investigation (Manufacturer: Fortelab Indústria de Fornos Elétricos Ltda-ME, São Carlos, Brazil). Fine type K thermocouples, made of 0.2 mm diameter wires and sheathed in stainless steel tubes of 1.6 mm diameter, are inserted from the side into the stainless steel mold. In order to determine temperatures and their changes over time (i.e., the thermal profiles) along with solidification, the thermocouples were spread in strategic positions along the mold length. Due to the fineness of the thermocouples, minor displacements which occur have been detected thanks to post-mortem tests. As such, exact location of the tips of the thermocouples could be determined. Each of the examined alloys was molten, poured into the mold, and reheated to 3% above the *liquidus* temperature before solidification could be initiated.

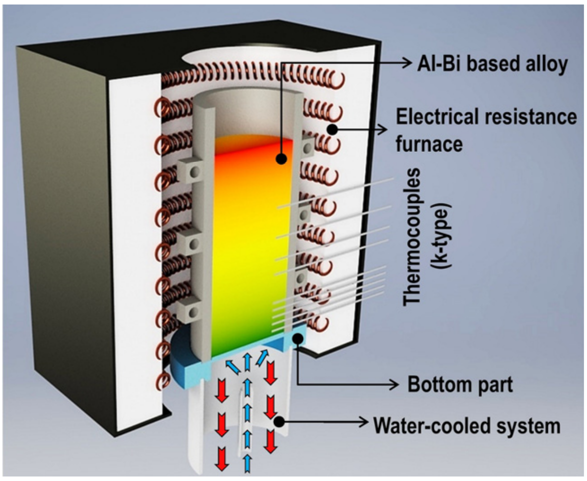

Figure 1. Solidification furnace used for producing directionally solidified (DS) castings.

The inner lateral surface of the mold was coated with alumina, having a 3 mm thick bottom plate of SAE 1020 steel (ArcelorMittal Brasil, Belo Horizonte, Brazil) closing the base of the mold. This plate surface has been uniformed with a 1200 grit sandpaper finish. In the directional solidification apparatus, in which inside temperatures can be controlled by radial electrical wiring, the cylindrical stainless-steel mold was placed so that the molten alloy could be reheated after pouring. With the start of the cooling water activation at the bottom and the beginning of solidification from the bottom up, the thermal profiles could be evaluated and recorded.

Microstructures formed in several regions along the solidified casting with respect to each tested alloy were characterized. The goal is to assess the microstructure, to measure the Bi spacing and the Bi diameter, as well as linking these parameters with the cooling rate according to the different positions in the casting and to a certain alloy tested. Additional experimental details can be found in previous studies [27].

Cross-sections of the casting have been polished and etched with a solution of 0.5 per cent hydrofluoric acid (HF) in water in order to expose the microstructure. Hence, micrographs could be assessed using an optical microscope (Olympus Corporation, GX41 model, Tokyo, Japan). Bi droplets found in the Al matrix have been quantified using image processing systems. They made it possible to count either the diameter (d) of the Bi droplets or the interphase spacing (λ_{Bi}). At least 50 readings for d and 50 readings for λ_{Bi} were performed for each examined position along the length of each casting. By averaging the horizontal distances between the centers of neighboring droplets, the spacing between Bi droplets was calculated.

X-ray diffraction (XRD) data of some samples along the length of the DS castings were collected by using a diffractometer (Bruker Corporation, D8 Advance ECO model, Fremont, CA, USA) with Cu Kα (λ = 1.54056 Å). Within a general 5–90° range, 2-theta reflections' selection was carried out mainly to identify Bi, α-Al, and intermetallic phases. Micro-adhesive wear tests were conducted on transverse samples from several positions along the length of the DS Al-Bi, Al-Bi-Zn, and Al-Bi-Cu alloys castings. An AISI 52100 bearing steel (Villares Metals, Sumare, Brazil) sphere with a diameter of 25.4 mm was rotated against the sample during the wear tests, generating a wear crater. Volume (V) of the generated crater was determined after contact between the steel sphere and the sample, through the application of a normal contact load of 0.9 N by the sample. The imposed sliding speed was 0.33 ms^{-1} (250 rpm). After wear tests, using a Field Emission Gun (FEG)—Scanning Electron Microscopy/Energy Dispersive X-Ray Spectroscopy (SEM/EDS) instrument (Field Electron and Ion Company, FEI, Hillsboro, OR, USA), the worn surface morphologies were evaluated.

Average Bi spacing increases from bottom to top of the DS castings. As such, samples have been extracted along the length of the casting in order to allow a representative number of tensile specimens to be machined and tested, being associated with representative mean λ_{Bi} values. This implies that the continuous evolution of λ_{Bi} over the length of the DS casting is fitted with a step function in which a specific tensile specimen is associated with each step (i.e., each λ_{Bi}). Figure 2 shows the geometry of the tensile specimens. The specimens for the tensile tests were machined according to the requirements of the American Society for Testing and Materials (ASTM) E 8M/04. The tensile tests were conducted on an instrument with adequate load capacity (Instron, Norwood, MA, USA).

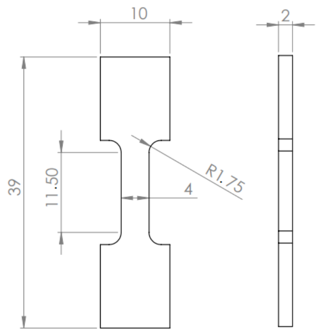

Figure 2. Tensile test specimen geometry. All dimensions are in mm.

3. Results and Discussion

By analyzing the thermal profiles of each alloy during directional solidification, it was possible to determine the solidification thermal parameters: cooling rate and growth velocity. The *liquidus* temperatures were determined experimentally by means of controlled and slow cooling curves. From that, power functions represented the experimental plots of thermocouple location (P) as a function of time of passage (t) of the *liquidus* solidification front by each thermocouple. Thus, the following function was determined for each alloy:

$$P(t) = a \times (t)^b \tag{1}$$

where a and b, are constants. The time derivatives of these functions resulted in v_L. Furthermore, the method of data acquisition used provided for the precise determination of the slope of the experimental thermal profiles immediately after the *liquidus* isotherm passage, determining the cooling rate, $\dot{T}_L$.

Variation in the solidification-cooling rate, $\dot{T}_L$, can be considered roughly unique when the experimental points of the three tested alloys are evaluated together according to Figure 3a. On the other hand, the growth rates, v_L, associated with the *liquidus* isotherm displacement proved to be different when comparing the three alloys between them, as showed in Figure 3b. In this sense, the addition of a third element (both Cu and Zn) caused an increase in the growth rate.

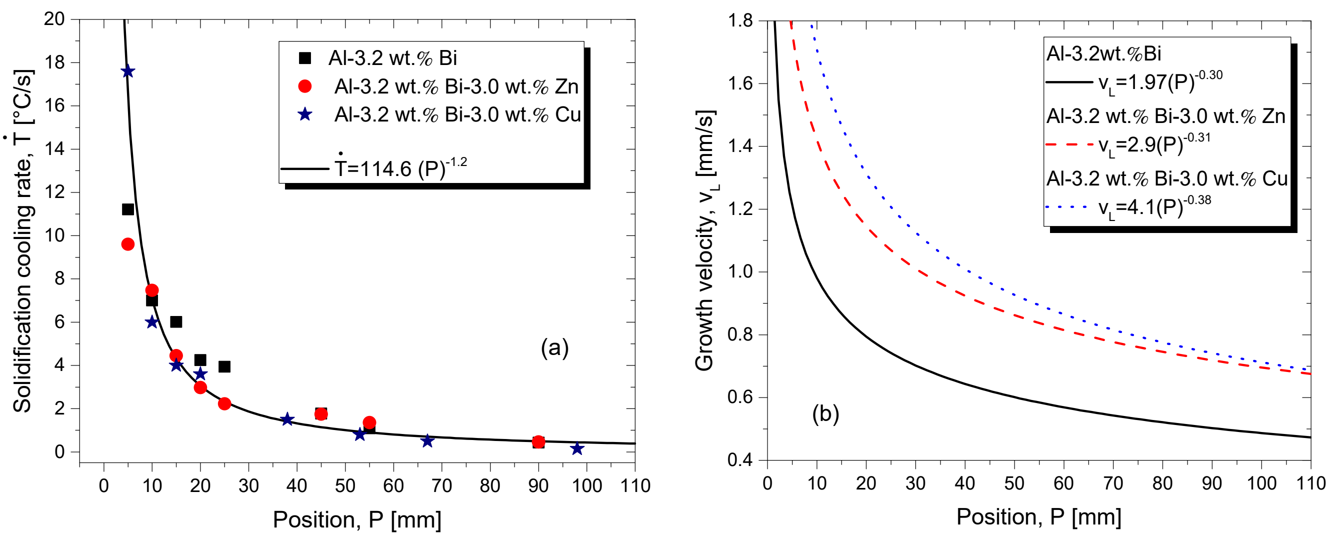

Figure 3. Experimental variations of (**a**) solidification cooling rates and (**b**) growth rates along the casting length of the evaluated Al-Bi(-Cu,-Zn) alloys.

If the position at 10 mm from the metal-mold interface is considered in Figure 3b, the growth velocity of the alloy containing Cu is 80% higher than that of the alloy without addition. This means almost twice as much, which can interfere with either the Bi spacing or its morphology. Ratke et al. [18] and Silva et al. [9] demonstrated a strong dependence on the distribution of Bi with the growth velocity.

Plots of interest include relating a microstructural parameter (in this specific case, λ_{Bi} and d_{Bi}) to a thermal parameter of the solidification process, that is, the cooling rate. These process charts are important for controlling the size and distribution of Bi, in addition to providing a comparative perspective between the three Al-Bi-X evaluated alloys, as can be observed in Figure 4.

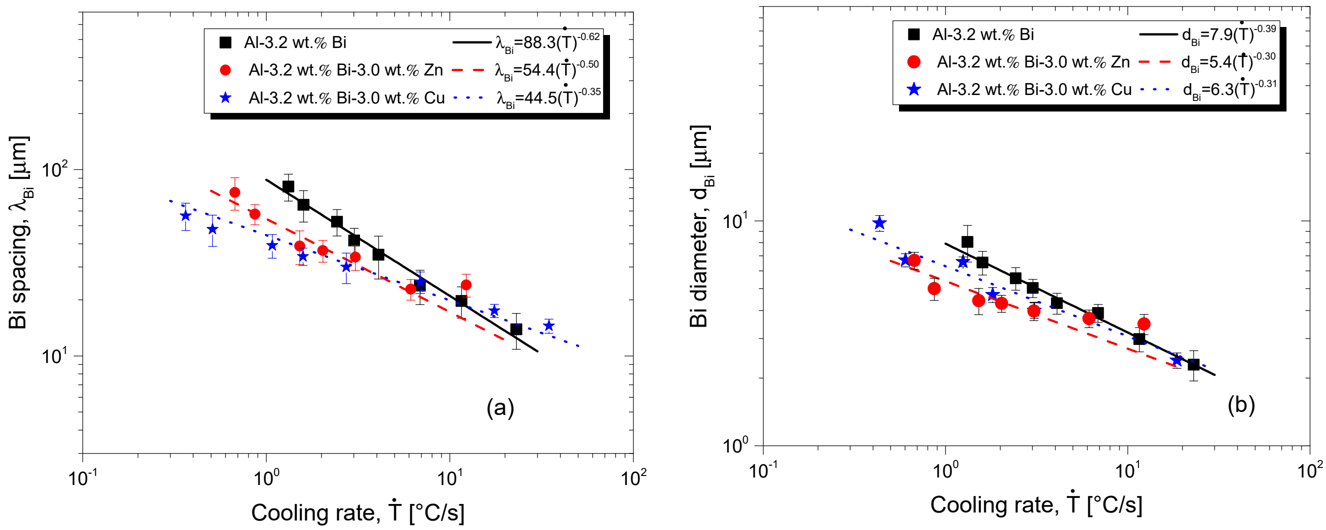

Figure 4. (**a**) Spacing between Bi droplets and (**b**) Bi diameter varying with cooling rate for the Al-3.2 wt.% Bi (squares symbols), Al-3.2 wt.% Bi-3.0 wt.% Zn (circles symbols), and Al-3.2 wt.% Bi-3.0 wt.% Cu (stars symbols) alloys.

Due to the difference in the power-function exponents found for representing each alloy, the evaluation can be divided into two phases. Firstly, for solidification cooling rates greater than 6.0 K/s, it appears that the addition of a third element has little or no effect on Bi spacing or Bi diameter. Secondly, for lower cooling rates (<6.0 K/s), both Cu and Zn influence by reducing λ_{Bi} and d_{Bi}. Therefore, both Zn and Cu resulted in a positive microstructural refining effect. It can be inferred that Cu and Zn affected the formation of the Bi droplets in the sense that the contact of the added elements may increase the nucleation rate of the minority phase, as demonstrated elsewhere [22–24]. Higher growth rates related to the Al-3.2 wt.% Bi-3.0 wt.% Zn and Al-3.2 wt.% Bi-3.0 wt.% Cu alloys also justify the resulting microstructures as being more refined.

As can be seen in Figure 5, columnar grains have evolved in the opposite direction to that of heat extraction, forming the macrostructures of the Al-Bi(-X) alloys. In all castings, there was essentially columnar grain growth, with the presence of few equiaxial grains closest to the top of the castings. Therefore, the morphology of the grains in the examined alloys samples is usually columnar. Furthermore, microstructures at different points are shown in Figure 5. The regions associated with the microstructures are those indicated by the vertical lines from the macrostructures. The chosen positions show the microstructural differences in two regions of the casting, that is, closer to the refrigerated surface (bottom) and therefore corresponding to higher solidification rates, and more distant, that is, grown at lower solidification rates. It can be seen that the Bi particles are larger for regions further away from the base of the casting (i.e., for regions with a lower cooling rate).

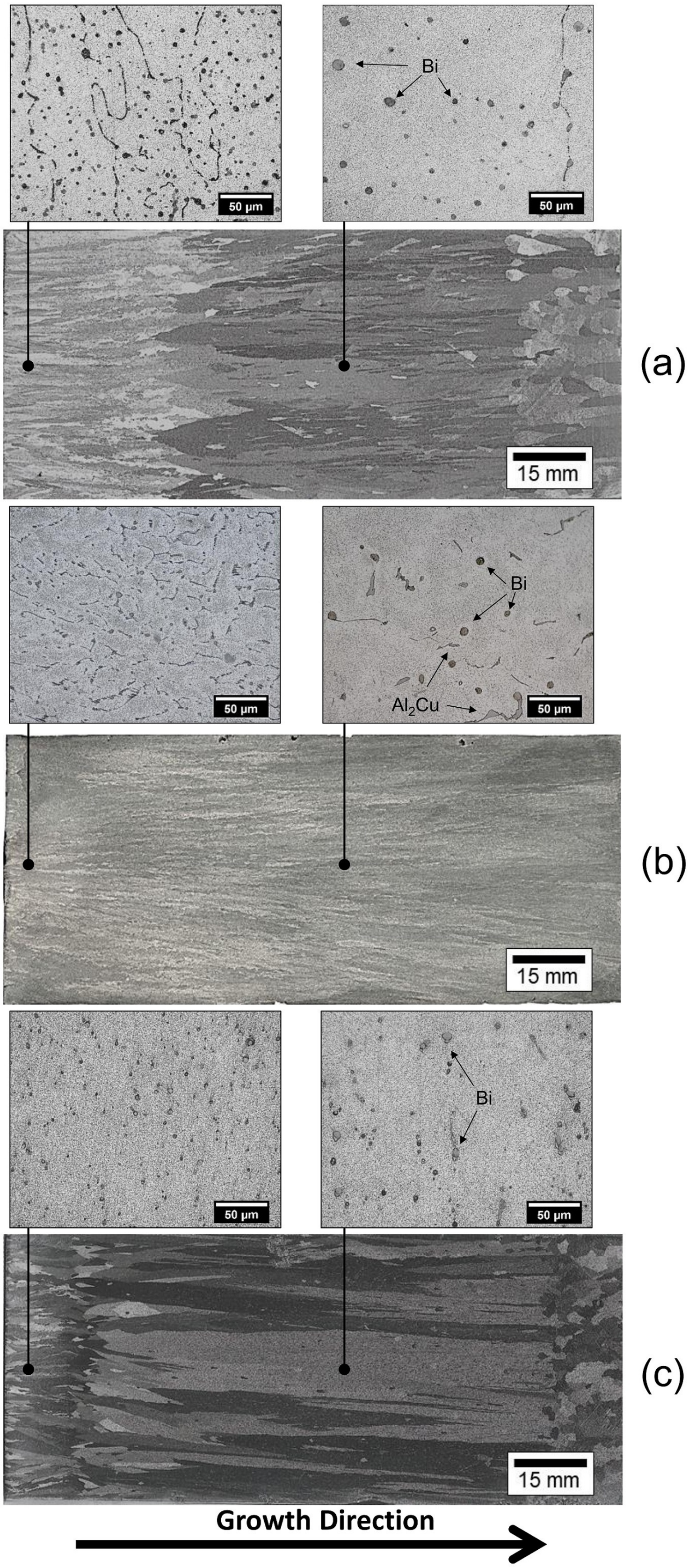

Figure 5. Macrostructures and respective microstructures at 2 points along the length of the directionally solidified (DS) (**a**) Al-3.2 wt.% Bi, (**b**) Al-3.2 wt.% Bi-3.0 wt.% Cu, and (**c**) Al-3.2 wt.% Bi-3.0 wt.% Zn alloys castings.

Due to the proximity of microstructural refining conditions (cooling rates higher than 10 K/s), samples from positions closest to the refrigerated surface of the DS castings were chosen for XRD decoding. As expected, the α-Al and Bi phase's reflections prevailed along the indexes of the patterns in Figure 6. Zn phases could not be distinguished. Zn is probably in solid solution due to the non-equilibrium conditions under which solidification of the Al-3.2 wt.% Bi-3.0 wt.% Zn alloy was performed. This could preserve Zn atoms saturated within the α-Al matrix. Besides that, the solubility of Zn in Al is quite high, as reported by Mondolfo [28].

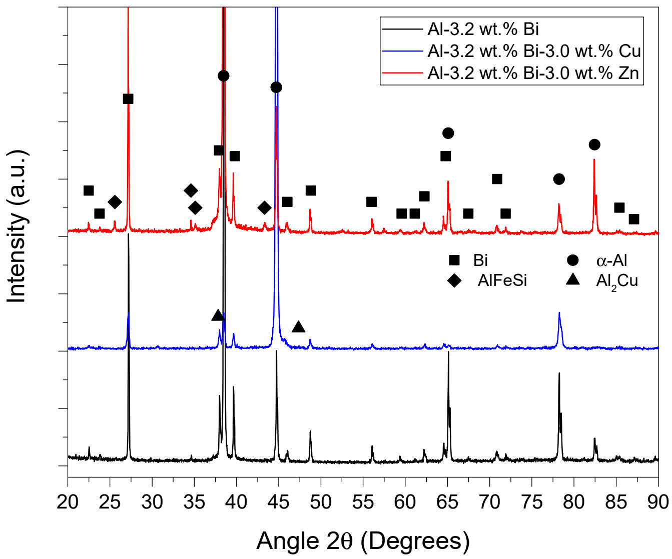

Figure 6. X-ray diffraction patterns performed on the Al-3.2 wt.% Bi, Al-3.2 wt.% Bi-3.0 wt.% Cu, and Al-3.2 wt.% Bi-3.0 wt.% Zn alloys samples solidified at cooling rates higher than 10 K/s.

Phases, such as Al_2Cu and AlFeSi, have also been identified. The AlFeSi phase originates from the presence of Si and iron (Fe) impurities in the elements used in the preparation of the alloys. Small peaks of Al_2Cu arise from the nucleation of this phase in the course of solidification of the Al-Bi-Cu alloy. The low intensity peaks suggest that the reaction $L_{Al} \rightarrow Al_2Cu + (Al) + L_{Bi}$ occurred only partially in the Al-3.2 wt.% Bi-3.0 wt.% Cu alloy during solidification, thanks to the relative high solubility of Cu in the Al-rich phase, although this reaction could be expected due to the proximity to the Al-Bi side when analyzing the ternary Al-Bi-Cu alloy [29,30].

Results showing representative stress-strain curves of the three Al-Bi(-X) alloys for samples exposed to different cooling conditions are shown in Figure 7. The samples positions at 6, 48, and 90 mm represent conditions of fast, intermediate and slow solidification inside an experimental range of cooling rates from 0.5 to 15 K/s. It is also noted that the addition of Zn and Cu reduced the elongation at fracture, even with the resulting better distribution of Bi. This seems to be associated with the interaction of the third elements with the Bi droplets. On the other hand, only the addition of Cu was effective in terms of improving tensile strength. It appears to be associated with the formation of a highly strengthened Al-rich matrix containing Cu, in addition to the Al_2Cu presence. In contrast, hardening of the matrix enriched in Al was not effective in the case of the addition of Zn.

The addition of Cu has shown to be efficient in promoting hardening by solid solution as demonstrated by Maki et al. [20]. Another effective hardening mechanism in the case of Cu addition in Al is the presence of a fraction of Al_2Cu constituting the microstructure, also recognized as a reinforcement phase [31].

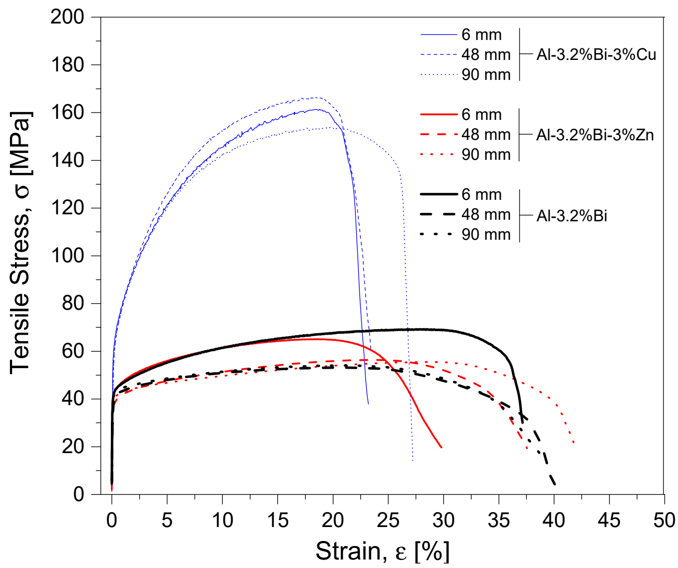

Figure 7. Stress-strain curves of tensile testing for the Al-3.2 wt.% Bi, Al-3.2 wt.% Bi-3.0 wt.% Zn, and Al-3.2 wt.% Bi-3.0 wt.% Cu alloys.

Figure 8 depict wear resistances (WR = 1/V) related to sliding distances of 798 m and 1197 m, respectively, as a function of λ_{Bi} for the Al-3.2 wt.% Bi, Al-3.2 wt.% Bi-3.0 wt.% Zn, and Al-3.2 wt.% Bi-3.0 wt.% Cu alloys. It is quite clear noting that the wear resistance of the alloy containing Cu is nearly double that of the other two alloys. Furthermore, wear resistance is improved in the case of samples having more refined microstructures, that is, lower λ_{Bi}. A finer distribution of the Bi minority phase promotes a better self-lubricating effect, reducing wear damage. For the alloys without addition and containing Zn, the wear behavior is quite similar, with some superiority for the Al-3.2 wt.% Bi-3.0 wt.% Zn alloy.

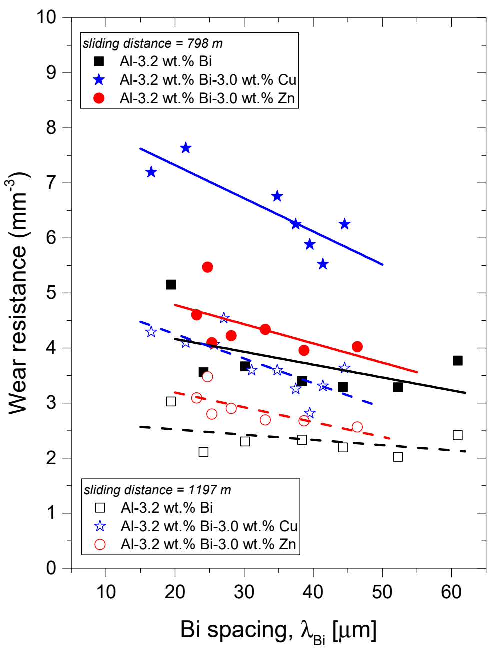

Figure 8. Wear resistance translated by the inverse of the worn out volume (V) as a function of the Bi spacing for either 798 or 1197 m of sliding distance related to the Al-Bi(-Cu,-Zn) alloys.

An interesting way to compare the tensile results and to investigate the influence of the microstructure is to plot graphs of the tensile properties as a function of of $\lambda_{Bi}{}^{-1/2}$, as those shown in Figure 9. Through these experimental trends, it is clear that not only the superior mechanical resistance (tensile strength) of the Al-Bi-Cu alloy in comparison with the others (see Figure 9a,b) but also the inefficiency of Zn added to the Al-3.2 wt.% Bi alloy, resulting in no changes in all the properties if considered the examined range of λ_{Bi}.

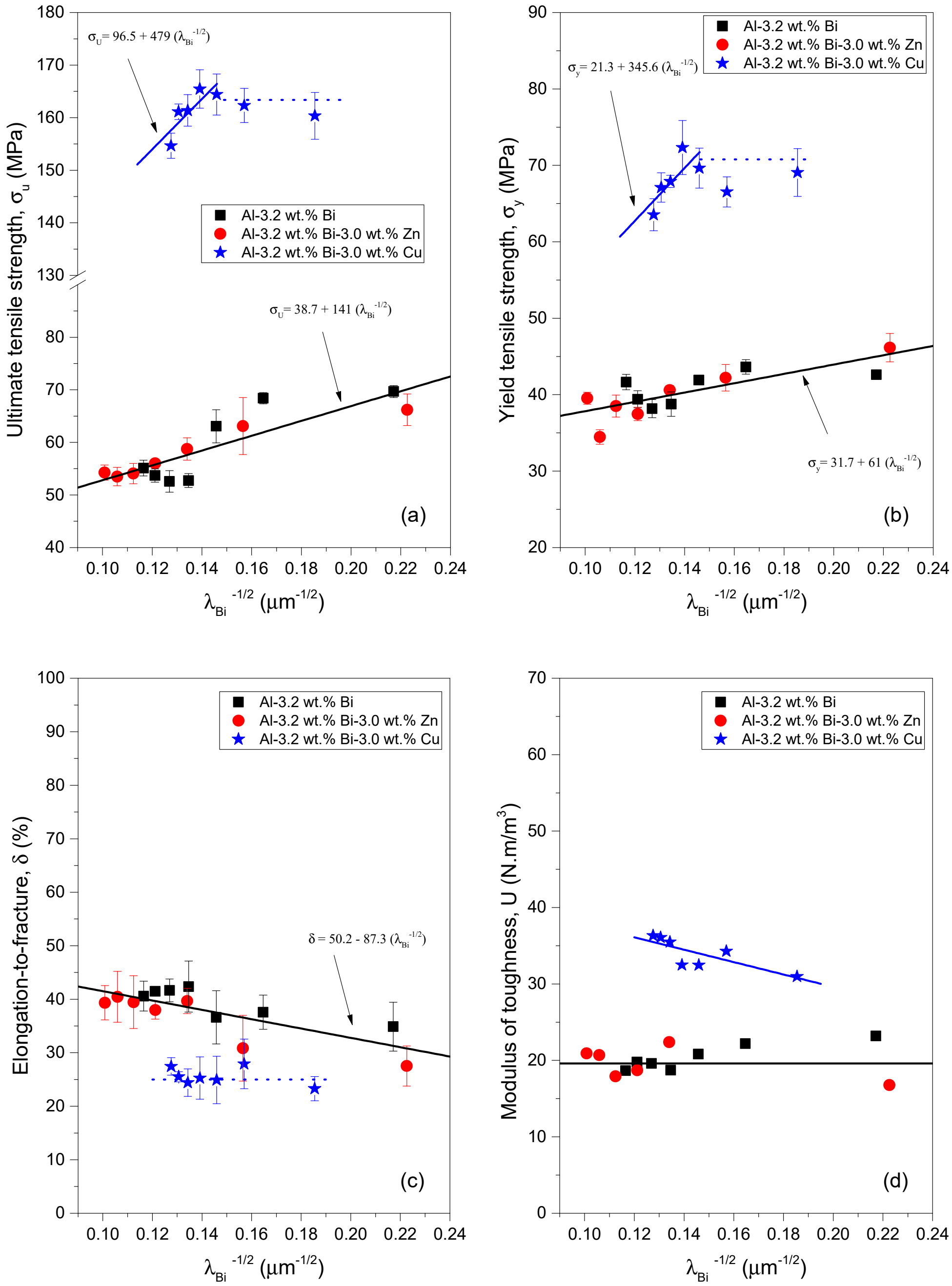

Figure 9. Tensile properties of the DS Al-Bi(-Cu,-Zn) alloys: (**a**) σ_u vs. $\lambda_{Bi}{}^{-1/2}$, (**b**) σ_y vs. $\lambda_{Bi}{}^{-1/2}$, (**c**) δ vs. $\lambda_{Bi}{}^{-1/2}$, and (**d**) U vs. $\lambda_{Bi}{}^{-1/2}$.

Variations in the tensile properties as a function of $\lambda_{Bi}{}^{-1/2}$ were mostly characterized by Hall-Petch-type relationships. The exception remained in elongation of the Al-Bi-Cu alloy and toughness of the Al-Bi and Al-Bi-Zn alloys. In these cases, due to little variability, horizontal constants representative of these behaviors were adopted.

In the analysis of Al-Sn alloys, also developed for sliding bearings and self-lubricating, Bertelli et al. [32] demonstrated that the addition of 10 wt.% Cu to the Al-20 wt.% Sn alloy provided an increase of up to 3 times in σ_u. Quite similarly, an increase in σ_u of the same order can be noticed by comparing the results of the Al-3.2 wt.% Bi and Al-3.2 wt.% Bi-3.0 wt.% Cu alloys.

By measuring the area under the stress-strain curve to the point of fracture, it was possible to determine the toughness, *U*. Figure 10 shows a joint plot of the application properties investigated so far for the Al-3.2 wt.% Bi-3.0 wt.% Cu alloy. While tensile strength and wear resistance show paired behavior in the trends in Figure 10, toughness and wear resistance evolve in the opposite way as a function of λ_{Bi}. It can be inferred that the reduction in toughness in the range in which it occurs for this alloy samples does not decisively affect the improvement of wear resistance, which depends largely on the tensile strength.

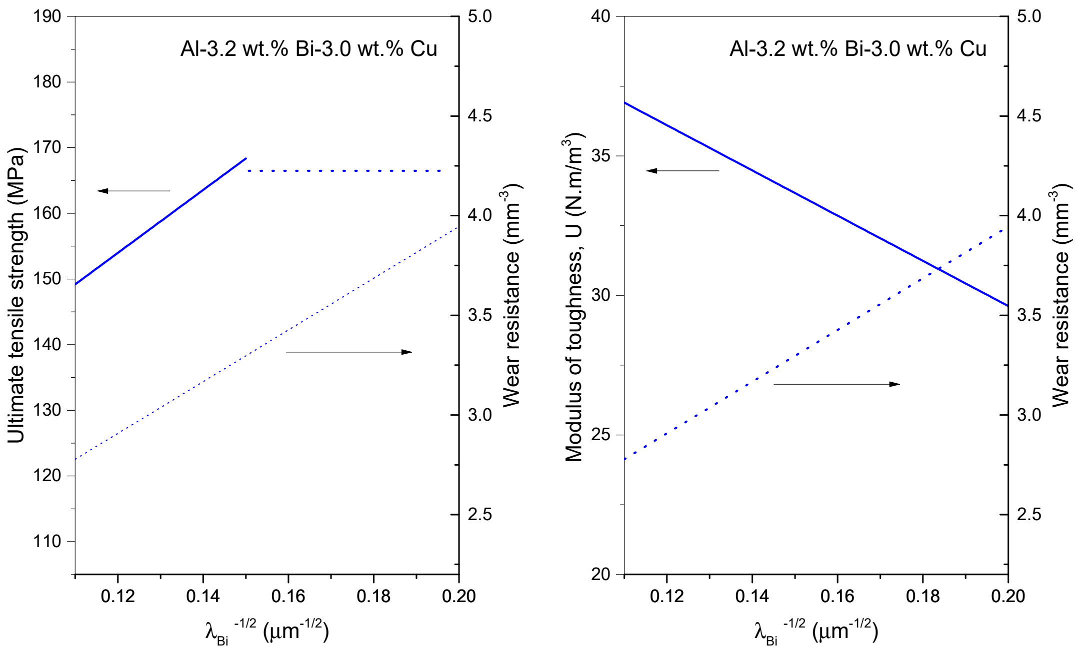

Figure 10. Mapping of the application properties obtained for wear analysis of the DS Al-Bi-Cu alloy.

Examples of wear surfaces of craters formed during the wear tests with the Al-Bi(-X) alloys are shown in Figure 11. Results related to two microstructural conditions, refined and coarse, were chosen for each alloy for comparative purposes. It should be noted that, for the Al-3.2 wt.% Bi and Al-3.2 wt.% Bi-3.0 wt.% Zn alloys, there was a predominance of adhesive wear mechanisms, resulting in expressive surface delamination due to the high levels of plastic deformation, as can be observed in Figure 11a,b. Lower toughness of these alloys' samples in the order of 20 N.m.m^{-3} facilitated the occurrence of material pullout failure. Because of the extreme plastic deformations, the higher toughness of the Al-Bi-Cu alloy samples tends to be able to minimize the detachment processes. As such, higher wear resistance is achieved. On the other side, a more scratched surface concurring with the sliding path was shown by fine and shallow grooves in the Al-3.2 wt.% Bi-3.0 wt.% Cu alloy (see Figure 11c).

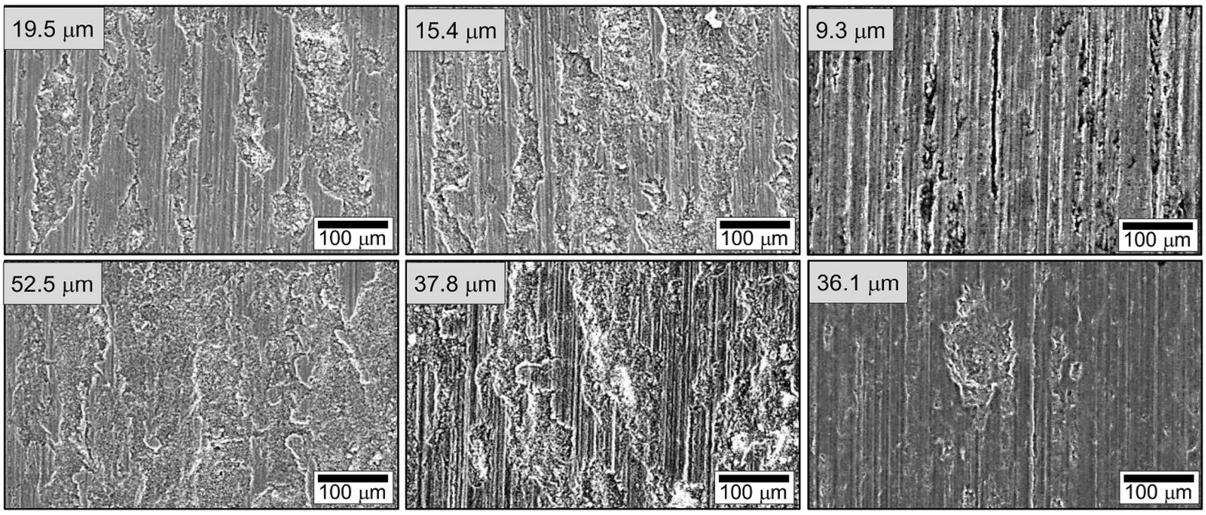

(a) (b) (c)

Figure 11. Typical SEM images of worn regions in the (**a**) Al-3.2 wt.% Bi, (**b**) Al-3.2 wt.% Bi-3.0 wt.% Zn, and (**c**) Al-3.2 wt.% Bi-3.0 wt.% Cu alloys (all images obtained after 60 min of wear test and values inside represent λ_{Bi} in µm).

Figure 12 shows SEM images of the fracture surfaces of some of the Al-Bi(-x) samples tested. Dimples triggered and formed around the soft Bi-rich particles characterized the fracture surfaces of the three alloys, suggesting a ductile fracture mode. Elevated elongation, similarly, leads to deep dimples. While the dimples are deeper for the Al-3.2 wt.% Bi and Al-3.2 wt.% Bi-3.0 wt.% Zn alloys, which means that these alloys are more ductile, shallower dimples have been formed for the Al-3.2 wt.% Bi-3.0 wt.% Cu alloy sample.

While the Al-3.2 wt.% Bi-3.0 wt.% Cu alloy samples were characterized by smaller λ_{Bi}, which can favor start of cracks and growth into large fracture dimples, their tensile strengths were higher than those of the other alloys. This is mainly because of the Al-rich matrix, which has its strength improved due to the Cu addition.

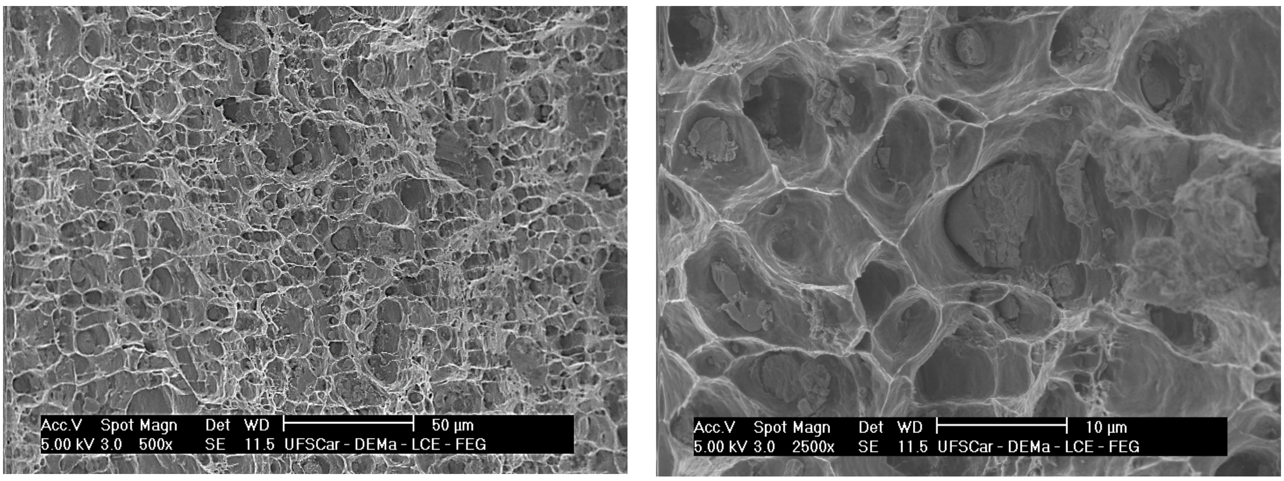

(**a**) (**b**)

Figure 12. *Cont.*

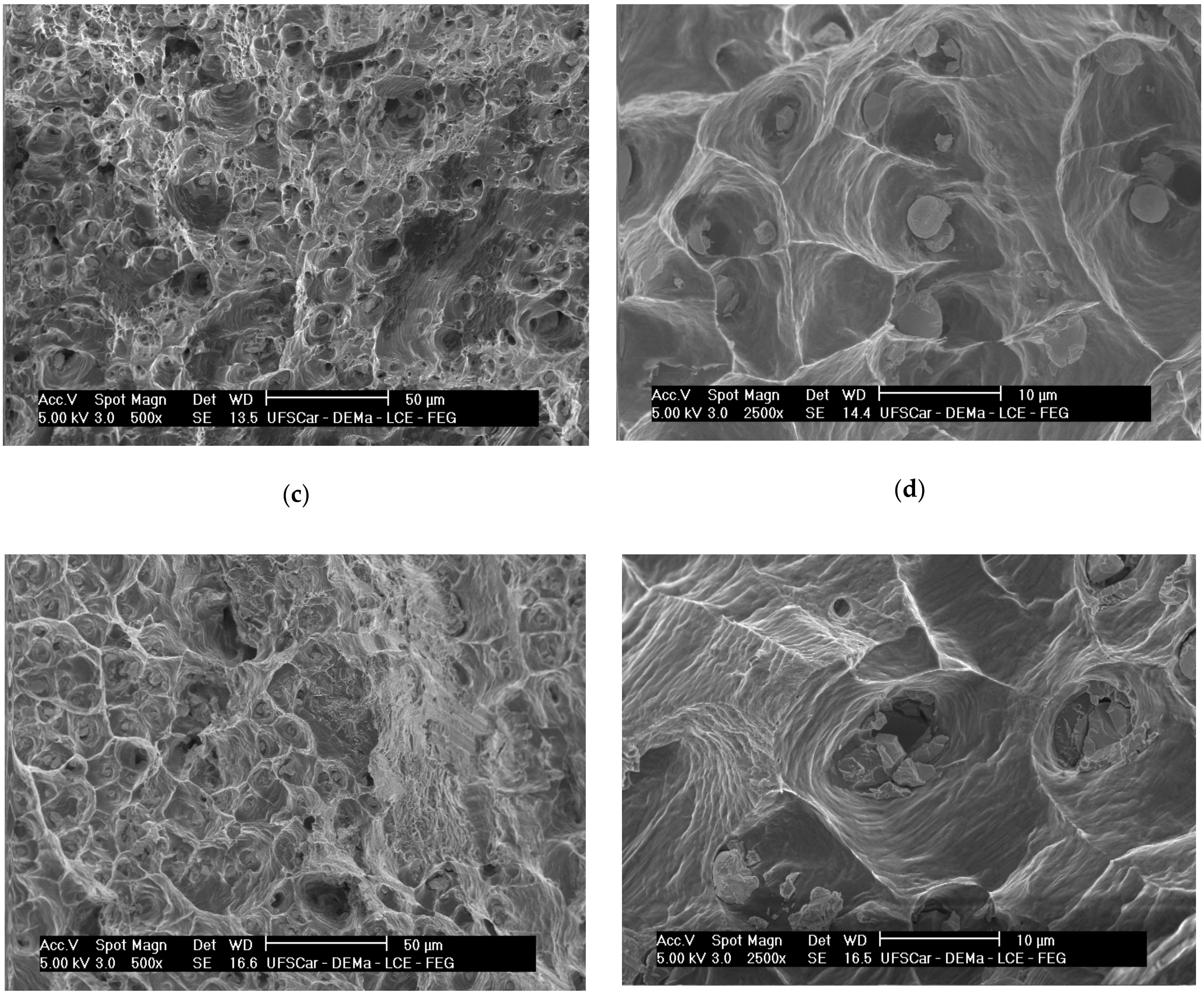

(**c**) (**d**)

(**e**) (**f**)

Figure 12. Fracture surfaces of the tensile-tested samples in two different magnifications: (**a**,**b**) Al-3.2 wt.% Bi, (**c**,**d**) Al-3.2 wt.% Bi-3.0 wt.% Zn, and (**e**,**f**) Al-3.2 wt.% Bi-3.0 wt.% Cu alloys.

4. Conclusions

Transient directional solidification processing has been successful in controlling the microstructure of an alternative Al-Bi-Cu alloy for sliding bearings. This was possible due to the control of the cooling rate achieving high tensile properties (ultimate tensile strength of 165 MPa and elongation of 27%), as well improved wear resistance. The results of the Al-3.2 wt.% Bi-3.0 wt.% Cu alloy are compatible with values of tensile strength obtained for bearing Al-Sn-Cu alloys, with ductility being higher compared to these alloys. These findings are important when considering increasing demands in new designs of sliding bearings. The following specific conclusions can be drawn:

- The solidification microstructures of the DS Al-3.2wt.% Bi- (3.0 wt.%Zn/3.0 wt.% Cu) alloys castings were shown to be formed essentially by a α-Al-rich matrix and Bi particles. For the Zn containing alloy, Zn phases could not be distinguished, since Zn is possibly in solid solution in Al due to the experimental non-equilibrium solidification conditions. For the Cu containing alloy, Cu is both in solid solution in Al and as in Al_2Cu. The spacing between Bi particles (λ_{Bi}) and Bi diameter (d_{Bi}), representing the length scale of the microstructure, have been correlated with the solidification cooling rate ($\dot{T}_L$) for any examined alloy. For lower cooling rates (<6.0 K/s), the additions of both Cu and Zn were shown to result in a positive microstructural refining effect, reducing λ_{Bi} and d_{Bi}.

- The tensile properties, i.e., ultimate (σ_u) and yield (σ_y) strengths and elongation at fracture (δ), were experimentally examined with respect to λ_{Bi} by analyzing samples of each alloy casting representing conditions of fast, intermediate, and slow solidification inside an experimental range of cooling rates from 0.5 to 15 K/s. Hall-Petch-type relationships relating σ_u, σ_y, and δ to ${\lambda_{Bi}}^{-1/2}$ have been derived. Only the addition of Cu was shown to be effective in terms of improving the tensile strength, whereas the additions of Zn and Cu reduced the elongation, even for the highest cooling rates that resulted in better distribution of Bi.
- The wear resistance (*WR*) of the studied alloys has been experimentally examined as a function of λ_{Bi}. It was shown that *WR* of the alloy containing Cu is nearly double that of the other two alloys, since a finer distribution of the Bi minority phase promotes a better self-lubricating effect, thus reducing wear damage.
- The area under the tensile stress-strain curve to the point of fracture, was also measured for the Al-3.2 wt.% Bi-3.0 wt.% Cu alloy, with a view to permitting the toughness, U, to be determined. A joint plot of the application properties, i.e., (σ_v and *WR*) vs. ${\lambda_{Bi}}^{-1/2}$ and (U and *WR*) vs. ${\lambda_{Bi}}^{-1/2}$ demonstrated that the reduction in U in the range in which it occurred for this alloy samples, does not decisively affect the improvement of wear resistance, which depends largely on the tensile strength.

Author Contributions: Conceptualization, J.E.S.; Analysis, R.A.V.R.; Writing-original draft preparation, R.A.V.R. and J.E.S.; Writing-review and editing, A.G.; Project administration, R.A.V.R. and J.E.S. All authors have read and agreed to the published version of the manuscript.

Funding: This research was funded by FAPESP—São Paulo Research Foundation, Brazil (grant 2019/23673-7), CNPq—National Council for Scientific and Technological Development, Brazil and CAPES—Coordenação de Aperfeiçoamento de Pessoal de Nível Superior, Brazil (Finance Code 001). And The APC was funded by CNPq - National Council for Scientific and Technological Development.

Data Availability Statement: The data presented in this study are available on request from the corresponding author. The data are not publicly available because pertain to a research still in development.

Conflicts of Interest: The authors declare no conflict of interest.

Abbreviations

Bi	Bismuth
Zn	Zinc
Cu	Copper
Al	Aluminum
wt.%	Weight %
v_L	Growth rate or growth velocity
Si	Silicon
DS	Directionally Solidified
SAE	Society of Automotive Engineering
λ_{Bi}	Bi spacing
d_{Bi}	Bi diameter
HF	Hydrofluoric acid
AISI	American Iron and Steel Institute
V	Volume
N	Newton
rpm	Rotation per minute
FEG	Field Emission Gun
SEM	Scanning Electron Microscopy

EDS	Energy Dispersive X-Ray Spectroscopy
ASTM	American Society for Testing and Materials
P	Position from the metal-mold interface
t	time of passage of the *liquidus* solidification front
$\dot{T}_L$	Solidification cooling rate
XRD	X-ray diffraction
Fe	Iron
L	Liquid
a.u.	Arbitrary unit
σ	Tensile stress
ε	Strain
WR	Wear resistance
σ_u	Ultimate tensile strength
σ_y	Yield tensile strength
δ	Elongation-to-fracture
U	Toughness

References

1. Schaffer, P.L.; Mathiesen, R.H.; Arnberg, L.; Di Sabatino, M.; Snigirev, A. In situ investigation of spinodal decomposition in hypermonotectic Al-Bi and Al-Bi-Zn alloys. *New J. Phys.* **2008**, *10*, 053001. [CrossRef]
2. Schaffer, P.L.; Mathiesen, R.H.; Arnberg, L. L2 droplet interaction with α-Al during solidification of hypermonotectic Al-8 wt.% Bi alloys. *Acta Mater.* **2009**, *57*, 2887–2895. [CrossRef]
3. Ran, G.; Zhou, J.E.; Xi, S.; Li, P. Microstructure and morphology of Al-Pb bearing alloy synthesized by mechanical alloying and hot extrusion. *J. Alloys Compd.* **2006**, *419*, 66–70. [CrossRef]
4. Gröbner, J.; Schmid-Fetzer, R. Phase transformations in ternary monotectic aluminum alloys. *JOM* **2005**, *57*, 19–23. [CrossRef]
5. Wang, N.; Wei, B. Phase separation and structural evolution of undercooled Fe-Sn monotectic alloy. *Mater. Sci. Eng. A* **2003**, *345*, 145–154. [CrossRef]
6. Freitas, E.S.; Spinelli, J.E.; Casteletti, L.C.; Garcia, A. Microstructure-wear behavior correlation on a directionally solidified Al-In monotectic alloy. *Tribol. Int.* **2013**, *66*, 182–186. [CrossRef]
7. Phanikumar, G.; Dutta, P.; Galun, R.; Chattopadhyay, K. Microstructural evolution during remelting of laser surface alloyed hyper-monotectic Al-Bi alloy. *Mater. Sci. Eng. A* **2004**, *371*, 91–102. [CrossRef]
8. Kumar Sharma, D.; Filipponi, M.; Di Schino, A.; Rossi, F.; Castaldi, J. Corrosion behaviour of high temperature fuel cells: Issues for materials selection. *Metalurgija* **2019**, *58*, 347–351.
9. Silva, A.P.; Spinelli, J.E.; Garcia, A. Thermal parameters and microstructure during transient directional solidification of a monotectic Al-Bi alloy. *J. Alloys Compd.* **2009**, *475*, 347–351. [CrossRef]
10. Majumdar, B.; Chattopadhyay, K. Aligned monotectic growth in unidirectionally solidified Zn-Bi alloys. *Metall. Mater. Trans. A Phys. Metall. Mater. Sci.* **2000**, *31*, 1833–1842. [CrossRef]
11. Battezzati, L.; Curiotto, S.; Johnson, E.; Pryds, N.H. Undercooling and demixing in rapidly solidified Cu-Co alloys. *Mater. Sci. Eng. A* **2007**, *449–451*, 7–11. [CrossRef]
12. Wang, J.; Ding, F.; Shen, W.; Li, T.; Wang, G.; Zhao, J. Thermal behavior of Cu-Co bimetallic clusters. *Solid State Commun.* **2001**, *119*, 13–18. [CrossRef]
13. Jiang, H.X.; Zhao, J.Z. Solidification of Immiscible Alloys Under the Effect of Electric and Magnetic Fields. *Acta Metall. Sin. Lett.* **2018**, *31*, 1240–1248. [CrossRef]
14. Zheng, T.X.; Zhong, Y.B.; Lei, Z.S.; Ren, W.L.; Ren, Z.M.; Debray, F.; Beaugnon, E.; Fautrelle, Y. Effects of high static magnetic field on distribution of solid particles in BiZn immiscible alloys with metastable miscibility gap. *J. Alloys Compd.* **2015**, *623*, 36–41. [CrossRef]
15. Silva, A.P.; Garcia, A.; Spinelli, J.E. Microstructure morphologies during the transient solidification of hypomonotectic and monotectic Al-Pb alloys. *J. Alloys Compd.* **2011**, *509*, 10098–10104. [CrossRef]
16. MAHLE GmbH. Bearings. In *Cylinder Components Properties, Applications, Materials*; Vieweg+Teubner: Wiesbaden, Germany, 2010; pp. 49–68. [CrossRef]
17. Ratke, L.; Diefenbach, S.; Drees, S.; Alkemper, J.; Prinz, B.; Romero, A.; Ahlborn, H. Multi-droplet Marangoni motion in immiscible AlSiBi alloys—Results of a D-2 experiment. *Adv. Space Res.* **1995**, *16*, 185–190. [CrossRef]
18. Ratke, L. Theoretical considerations and experiments on microstructural stability regimes in monotectic alloys. *Mater. Sci. Eng. A* **2005**, *413–414*, 504–508. [CrossRef]
19. Lamrous, D.; Debili, M.Y.; Boehm-Courjault, E. Microstructure and phase composition of Al-Zn alloys. *J. Adv. Microsc. Res.* **2013**, *8*, 266–269. [CrossRef]
20. Maki, K.; Ito, Y.; Matsunaga, H.; Mori, H. Solid-solution copper alloys with high strength and high electrical conductivity. *Scr. Mater.* **2013**, *68*, 777–780. [CrossRef]

21. Kumar, J.; Singh, D.; Kalsi, N.S.; Sharma, S.; Pruncu, C.I.; Pimenov, D.Y.; Rao, K.V.; Kapłonek, W. Comparative study on the mechanical, tribological, morphological and structural properties of vortex casting processed, Al–SiC–Cr hybrid metal matrix composites for high strength wear-resistant applications: Fabrication and characterizations. *J. Mater. Res. Technol.* **2020**, *9*, 13607–13615. [CrossRef]
22. Man, T.; Zhang, L.; Xu, N.; Wang, W.; Xiang, Z.; Wang, E. Effect of Rare-Earth ce on macrosegregation in Al-Bi immiscible alloys. *Metals* **2016**, *6*, 177. [CrossRef]
23. Jia, P.; Zhang, J.; Geng, H.; Teng, X.; Zhao, D.; Yang, Z.; Wang, Y.; Hu, S.; Xiang, J.; Hu, X. High-Efficiency Inhibition of Gravity Segregation in Al–Bi Immiscible Alloys by Adding Lanthanum. *Met. Mater. Int.* **2018**, *24*, 1262–1274. [CrossRef]
24. Man, T.; Zhang, L.; Xiang, Z.; Wang, W.; Huang, M.; Wang, E. Improvement of Microstructure and Wear Property of Al–Bi Alloys by Nd Addition. *JOM* **2018**, *70*, 1344–1348. [CrossRef]
25. Yang, Q.; Sun, Z.; Wang, Z. Effects of Sn, Si, and Cu addition on the microstructure and properties of hypermonotectic Al 92 Bi 8 alloy. *Mater. Sci. Eng. A* **2019**, *756*, 71–81. [CrossRef]
26. Pereira, C.L.; Gomes, L.F.; Spinelli, J.E. Effects of Bi addition on Si features, tensile properties and wear resistance of hypereutectic Al-15Si alloy. *IOP Conf. Ser. Mater. Sci. Eng.* **2020**, *861*. [CrossRef]
27. Oliveira, R.; Kakitani, R.; Ramos, L.R.; Gonçalves, D.L.; Garcia, A.; Cheung, N. The Roles of Mn and Ni Additions to Fe-Contaminated Al in Neutralizing Fe and Stabilizing the Cellular α-Al Microstructure. *J. Sustain. Metall.* **2019**, *5*, 561–580. [CrossRef]
28. Mandolfo, L.F. *Aluminum Alloys: Structure and Properties*, 1st ed.; Butterworth: Oxford, UK, 1976.
29. Mirković, D.; Gröbner, J.; Kaban, I.; Hoyer, W.; Schmid-Fetzer, R. Integrated approach to thermodynamics, phase relations, liquid densities and solidification microstructures in the Al–Bi–Cu system. *Int. J. Mater. Res.* **2009**, *100*. [CrossRef]
30. Kattner, U.R.; Burton, B.P. The Al-Bi-Cu System. *J. Phase Equilibria* **1992**, *13*, 629–635. [CrossRef]
31. Shabestari, S.G.; Moemeni, H. Effect of copper and solidification conditions on the microstructure and mechanical properties of Al–Si–Mg alloys. *J. Mater. Process. Technol.* **2004**, *153–154*, 193–198. [CrossRef]
32. Bertelli, F.; Freitas, E.S.; Cheung, N.; Arenas, M.A.; Conde, A.; de Damborenea, J.; Garcia, A. Microstructure, tensile properties and wear resistance correlations on directionally solidified Al-Sn-(Cu; Si) alloys. *J. Alloys Compd.* **2017**, *695*, 3621–3631. [CrossRef]